Structural and Dynamic Characterization of a Neuron-Specific Protein Kinase C Substrate, Neurogranin†

Xiaoyuan Ran,[⊥,§] Hong-Hua Miao,[‡,§] Fwu-Shan Sheu,*[,#] and Daiwen Yang*[,⊥]

Department of Biological Sciences, and Department of Chemistry, Department of Biological Sciences and the University Scholars Program, National University of Singapore, 14 Science Drive 4, Singapore 117543, Shanghai Institute of Biochemistry and Cell Biology, Chinese Academy of Sciences, Shanghai 200031, China

Received November 14, 2002; Revised Manuscript Received February 27, 2003

ABSTRACT: Neurogranin/RC3 is a neuron-specific, Ca^{2+}-sensitive calmodulin binding protein and a specific protein kinase C substrate. Neurogranin may function to regulate calmodulin levels at specific sites in neurons through phosphorylation at serine residue within its IQ motif, oxidation outside the IQ motif, or changes in local cellular Ca^{2+} concentration. To gain insight into the functional role of neurogranin in the regulation of calmodulin-dependent activities, we investigated the structure and dynamics of a full-length rat neurogranin protein with 78 amino acids using triple resonance NMR techniques. In the absence of calmodulin or PKC, neurogranin exists in an unfolded form as evidenced by high backbone mobility and the absence of long-range nuclear Overhauser effect (NOE). Analyses of the chemical shifts $^{13}C_\alpha$, $^{13}C_\beta$, and $^1H_\alpha$ reveal the presence of a local α-helical structure for the region between residues G25−A42. Three-bond $^1H_N-^1H_\alpha$ coupling constants support the finding that the sequence between residues G25 and A42 populates a non-native helical structure in the unfolded neurogranin. Homonuclear NOE results are consistent with the conclusions drawn from chemical shifts and coupling constants. ^{15}N relaxation data indicate motional restrictions on a nanosecond time scale in the region from D15 to S48. Spectral densities and order parameters data further confirm that the unfolded neurogranin exists in conformation with residual secondary structures. The medium mobility of the nascent helical region may help to reduce the entropy loss when neurogranin binds to its targets, but the complex between neurogranin and calmodulin is not stable enough for structural determination by NMR. Calmodulin titration of neurogranin indicates that residues D15−G52 of neurogranin undergo significant structural changes upon binding to calmodulin.

Neurogranin/RC3 (NG)[1] is a protein highly concentrated in the forebrain (*1*). It accumulates postsynaptically in dendritic spines of neurons (*2*). This protein acts as a messenger substrate of protein kinase C (PKC) that mediates molecular cascades during synaptic development and remodeling (*3*, *4*). NG is a member of the calpacitin protein family which includes other proteins such as neuromodulin (GAP-43), peptide protein 19 (PEP-19), Igloo and sperm protein 17 (SP17). Similar to other proteins of this family, NG binds calmodulin (CaM) in low Ca^{2+} environment and release CaM under high Ca^{2+} conditions (*5*), acting like a CaM capacitor (*1*). The Ca^{2+}-independent CaM-binding proteins in the family often possess a region that contains mainly basic and hydrophobic residues with a high propensity to form an amphipathic α-helix (*6*−*8*). This highly conserved region is referred to as the "IQ" motif (IQXXXRGXXXR) (*9*, *10*). It is considered to be the main structural and functional domain. Structural studies in conventional myosins have demonstrated that the IQ motif adopts an α-helical conformation that is stabilized by the CaM-related proteins (*11*, *12*). On the other hand, NG and GAP-43 are unfolded in vitro as found from CD spectroscopy studies (*8*, *13*). Upon binding to CaM in the absence of Ca^{2+}, an α-helix is induced within the CaM binding domain (IQ motif) and the helix may propagate to some residues in the N-terminal side of the IQ domain in both NG and GAP-43 (*8*). The stabilized helix may span from G25 to K47 in rat NG as found from the study of a number of overlapping peptides (*8*), where the sequence I_{33}QASFRGHMAR_{43} corresponds to the IQ motif. The serine residue (Ser-36 for Rat NG) in the IQ motif can be phosphorylated by PKC (*4*, *14*). The phosphorylation within the IQ domain lowers the binding affinity of NG for CaM (*4*, *5*, *15*); conversely, CaM binding attenuates PKC phosphorylation at the serine site within the IQ domain (*5*, *8*). Thus, NG and GAP-43 have been assumed to regulate postsynaptic and presynaptic CaM levels, respectively, via

† This work was supported through grants (R154-000-149-101 to D. W. Yang and R154-000-113-112 to F. S. Sheu) from the National University of Singapore.

* Corresponding authors, email addresses: dbsydw@nus.edu.sg (D. W. Yang) and dbssfs@nus.edu.sg (F. S. Sheu).

§ Both authors contributed equally to this work.

⊥ Department of Biological Sciences, and Department of Chemistry, National University of Singapore.

‡ Chinese Academy of Sciences.

Department of Biological Sciences and the University Scholars Program, National University of Singapore.

[1] Abbreviations: NG, neurogranin/RC3; CAM, calmodulin; GAP-43, neuromodulin; PKC, protein kinase C; LTP, long-term potentiation; LTD, long-term depression; NMR, nuclear magnetic resonance; CD, circular dichroism; EPR, electron paramagnetic resonance; T_1, longitudinal relaxation time; $T_{1\rho}$, rotating frame relaxation time; T_2, transverse relaxation time; NOE, nuclear Overhauser effect; TFE, trifluoroethanol; SDS, sodium dodecyl sulfate; EGTA, ethylene glycol bis(2-aminoethyl ether)-*N*,*N*,*N*′,*N*′-tetraacetic acid.

10.1021/bi0271751 CCC: $25.00
Published on Web 04/11/2003

PKC phosphorylation or changes in local cellular Ca^{2+} concentration.

PKC is an extrinsic membrane protein and phosphorylation of the PKC substrate is very likely to take place on the membrane surface (*16*, *17*). Before approaching PKC on the surface of the membrane the segment surrounding the phosphorylation site is considered to interact with the membrane in vivo. The study of a peptide corresponding to residues 28−43 of bovine NG (or A30−K45 of rat NG) using NMR, EPR, and CD spectroscopy indicated that an α-helix within the peptide is induced by association with SDS micelles and with vesicles containing phosphatidyl serine (*18*). Phosphorylation of NG is associated with long-term potentiation (LTP) and long-term depression (LTD). Therefore, it has also been proposed that NG and GAP-43 may play important roles in long-term potentiation (LTP) and neuroplasticity by releasing CaM through serine phosphorylation within the IQ motif (*1*, *19*).

Outside the IQ domain, NG contains four cysteine residues, which can be oxidized by nitric oxide and other oxidants to form intramolecular disulfide linkage(s) (*20*−*22*). On the other hand, NG and GAP-43 have been shown to regulate CaM-dependent nitric oxidate synthase activity through sequestration of CaM (*23*, *24*). CD studies show that modification of NG by oxidation forming disulfide does not affect the α-helical content of this protein in either water or TFE solution (*25*). However, oxidation of NG attenuates its binding affinity with CaM, indicating an alternative potential mechanism other than phosphorylation for the regulation of intracellular levels of CaM (*25*).

CaM can differentiate the unfolded NG from its modified forms and from other non-CaM binding proteins. Although there is no structural information to interpret the recognition mechanism, an important factor should be the apparent change in conformational entropy in most residues involved in the binding site (*26*, *27*). For such a system where folding and binding are coupled, the preference for an interaction can be increased without increase in binding affinity provided there is a compensational loss in conformational entropy (*28*, *29*). The weak or medium binding affinity of NG is favorable for the regulation of CaM-dependent activities through sequestration and release of CaM. Except for CaM and PKC, the reduced NG is also a substrate for phosphorylase kinase and may bind to membrane phospholipids (*17*, *30*). To understand more about the role of NG and other members of the calpacitin family of proteins in neurobiology, we have characterized the residual structure and dynamics of the reduced NG protein from rat (78 amino acids) using NMR techniques. The order parameters obtained from NMR relaxation allowed us to estimate the conformational entropy loss of the binding process.

MATERIALS AND METHODS

Expression and Purification of ^{15}N- and ^{13}C-Labeled NG. The construction of a bacterial expression vector containing the protein-coding region of rat NG cDNA has been reported previously (*31*). We used the same expression host of *Escherichia coli* BL21 (DE3)(pLysS) to express the stable isotope labeled NG for the present study. To express the ^{15}N- and ^{13}C-labeled NG, a single colony of the host strain was picked out from an agar plate grown overnight at 37 °C and then put into the ^{15}N- and ^{13}C-labeling medium. Each liter of isotope labeling medium contained 1× MOPS stock buffer, 1.32 mM K_2HPO_4, 50 mg of kanamycin, 1 g of $^{15}NH_4Cl$ and 2 g of ^{13}C-glucose. The 1× MOPS stock buffer contained 40 mM MOPS, 4 mM tricine, pH 7.4, 0.01 mM $FeSO_4$, 0.275 mM K_2SO_4, 0.5 mM $MgCl_2$, 50 mM NaCl, 0.5 μM $CaCl_2$, and was supplemented with 10 μM vitamins. The expression of NG was induced by adding 0.4 mM isopropyl-β-D-thio-galactoside (IPTG). The cells were grown for 6 h at 37 °C until cell density reached an O.D. 600 reading of around 0.8. The cells were harvested and then subjected to lysis for NG protein purification as described previously (*31*). CaM was prepared as described previously (*32*).

NMR Spectroscopy. NMR spectra were recorded at 500 MHz using a three-channel Bruker Avance spectrometer equipped with pulse field gradients. All the spectral data for NG were acquired at a protein concentration of 0.7 mM, pH 6.5, 50 mM KH_2PO_4 buffer, 5 mM DTT, at 25 °C. CaM titration was monitored by ^{1}H−^{15}N HSQC NMR at 25 °C. A total of 0.6 mg of CaM powder was taken each time and added directly to a protein solution containing 0.7 mM NG, 50 mM KH_2PO_4 buffer, 5 mM DTT, 5 mM EGTA at pH 6.5. The total CaM added was 15 mg, corresponding to a CaM/NG ratio of 2.5. Backbone resonance assignments were obtained using a number of triple resonance experiments, including HNCACB (*33*), CBCA(CO)NH (*34*), HN(CA)-CO, and HNCO (*35*). $^3J_{HN,H\alpha}$ coupling constants were measured using the HNHA pulse sequence (*36*). To obtain homonuclear NOEs, a 3D NOESY-HSQC (*37*) spectrum was recorded with a mixing time of 250 ms. An H(CCO)NH-TOCSY experiment was used to obtain proton chemical shifts (*38*). In all of the experiments, the proton spectral width in the direct observation dimension was 7000 Hz with 512 complex points. The spectral width in the indirect proton dimension was 5500 Hz for HNHA, NOESY-HSQC, and H(CCO)NH-TOCSY, with 64 complex points. A total of 16 complex points were recorded on the ^{15}N dimension using a spectral width of 1014 Hz, while 32 complex points were acquired for NOESY-HSQC. Forty complex points were recorded in ^{13}C dimension using spectral widths of 7000 Hz for CACB and 1250 Hz for CO, respectively. A relaxation delay of 1 s was used for all the experiments. The number of scans were 32 for NOESY-HSQC, 16 for HNCACB, CBCA(CO)NH, HN(CA)CO, and HNHA, and 8 for HNCO. The data were apodized with a sine weighting function shifted by 63° in the direct proton dimension and 81° in the indirect ^{1}H and ^{13}C dimensions. The ^{15}N time domain was doubled by linear prediction prior to the application of a cosine-squared window function. After zero filling and Fourier transformation the final data sets comprised of 1024, 256, and 128 points along the F3, F2, and F1 dimensions, respectively. Processing of the spectra was carried out using NMRPipe software (*39*). The spectra were analyzed using NMRView software.

The ^{15}N relaxation times T_1 and $T_{1\rho}$ and ^{1}H−^{15}N NOEs were measured by inverse-detected 2D NMR methods (*40*, *41*). Relaxation times T_1 were determined by collecting seven points with delays of 10, 90, 200, 300, 400, 500, and 600 ms using a recycle delay of 1 s and 8 scans. Relaxation times $T_{1\rho}$ were measured by collecting seven points with delays of 10, 30, 50, 80, 110, 140, and 170 ms using a spin-lock

power of 1 kHz, 2.5 s recycle delay and eight scans. To measure the heteronuclear NOEs, two spectra were acquired with and without proton saturation. Saturation was achieved by using a train of 120° ^{1}H pulses applied for 3 s after a 3 s recycle delay. All the data were recorded by using 96 and 512 complex points in t_1 and t_2 dimensions, respectively, and with spectral widths of 1014 Hz (^{15}N) and 7000 Hz (^{1}H).

Relaxation Data Analysis. Spin−spin relaxation time T_2 was calculated from $T_{1\rho}$ and T_1 according to

$$1/T_{1\rho} = 1/T_1 \sin^2\theta + 1/T_2 \cos^2\theta \quad (1)$$

where $\theta = \text{atan}(\Delta\omega/\omega_1)$, and $\Delta\omega$ and ω_1 are the resonance offset and spin-lock field strength, respectively. Relaxation data were analyzed using the reduced spectral density mapping approach. $J(0)$, $J(\omega_N)$, and $J(0.87\omega_H)$ were calculated using the following simplified equations (*42*):

$$1/T_1 = d^2/4[3J(\omega_N) + 7J(0.87\omega_H)] + c^2J(\omega_N) \quad (2)$$

$$1/T_2 = d^2/8[4J(0) + 3J(\omega_N) + 13J(0.87\omega_H)] + c^2/6[4J(0) + 3J(\omega_N)] \quad (3)$$

$$\text{NOE} = 1 + T_1(\gamma^H/\gamma^N)(d^2/4)[5J(0.87\omega_H)] \quad (4)$$

where $d = (\mu_0 h/8\pi^2)\gamma^H\gamma^N r_{NH}^{-3}$, $c = \omega_N(\sigma_{||} - \sigma_\perp)/\sqrt{3}$, γ is the gyromagnetic ratio, h is Planck's constant, μ_0 is the permeability of a vacuum, r_{NH} is the N−H bond length (1.02 Å), $\sigma_{||}$ and $\sigma_\perp$ are the parallel and perpendicular components of the assumed axial symmetric chemical shift tensor, and $\sigma_{||} - \sigma_\perp$ is taken as −170 ppm.

Recently, we have proposed and validated a simple method for obtaining order parameters from NMR relaxation data of both folded and unfolded proteins (*43*). The approach provides physically meaningful order parameters for even unfolded proteins, which has also been described by Schurr et al. and Alexandrescu & Shortle (*44*, *45*). The square of a generalized order parameter (S^2) is extracted from the fit of an individual residue using a simple Lipari-Szabo model (*46*):

$$J(\omega) = 0.4[S^2\tau_{loc}/(1 + \omega^2\tau_{loc}^2) + (1 - S^2)\tau_e/(1 + \omega^2\tau_e^2)] \quad (5)$$

where τ_{loc} is the apparent correlation time for a specific residue and τ_e is the effective correlation time that satisfies the relation $\tau_e \ll \tau_{loc}$.

RESULTS AND DISCUSSION

Resonance Assignments. Sequential assignment by standard triple resonance 3D experiments such as HNCACB and CBCA(CO)NH normally relies on the dispersion of $^{13}C_\alpha$, $^{13}C_\beta$, ^{15}N, and ^1H_N. Routine methods usually fail when the resonances are poorly dispersed, especially for $^{13}C_\alpha$, $^{13}C_\beta$, as in the case of NG. Fortunately, the chemical shift dispersion of carbonyl ^{13}C is still large enough in unfolded proteins. We have thus exploited the CO dispersions and used HNCO and HN(CA)CO together with HNCACB and CBCA(CO)NH to obtain the sequential assignment. Resonances for all nonproline residues were assigned; except the first five residues (M1−T5) due to their weak signals in the HSQC spectrum. Aliphatic proton resonance assignment was obtained from an H(CCO)-TOCSY spectrum. Figure 1 shows the assigned ^{1}H−^{15}N HSQC spectrum of rat NG protein. A couple of weak peaks in the glycine region (not labeled) are attributed to proline isomerization.

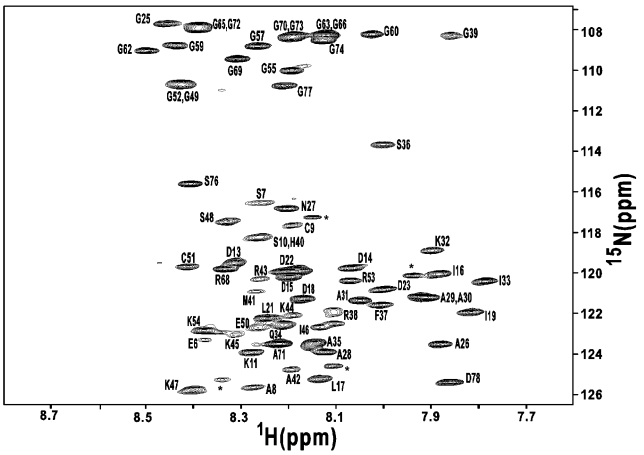

FIGURE 1: ^{1}H−^{15}N heteronuclear single quantum correlation spectrum (HSQC) of neurogranin recorded at 25 °C. The resonance assignments are indicated by amino acid names followed by residue numbers. Resonances resulting from impurities are indicated by asterisks (*).

Analysis of Chemical Shifts. $^{13}C_\alpha$, $^{13}C_\beta$, $^{13}C'$, and $^1H_\alpha$ chemical shifts are useful indicators of secondary structure in folded proteins (*47*, *48*). To identify residual structures in unfolded proteins, chemical shift deviations from random coil values for $^{13}C_\alpha$, $^{13}C_\beta$, $^{13}C'$, and $^1H_\alpha$ have to be calculated properly. We used random coil values derived from model peptides G−G−X−A−G−G at 1 M urea, pH 5 at 25 °C (*49*). The random coil shifts were further normalized to the values expected for the peptides G−G−X−G−G by taking into account the effect of alanine on the chemical shifts of residue X in the model peptides, i.e., 0.17 ppm for C_α and 0.03 ppm for H_α were added to the random coil shifts (*50*). Sequence dependent effects were corrected according to previously described methods (*50*). For nonproline residues, the effect of residue X on its neighboring residue Z is relatively small and can be approximated as the effect of residue X on residue G (glycine). Thus, the correction factors have been simply estimated from the chemical shift variation of glycine residues in peptides G−G−X−G−G relative to those in a peptide G−G−G−G−G (*50*). For proline residues, however, the correction factors are large and have to be calculated from other methods. The proline correction factor B for C_α was estimated from the chemical shift differences between the two sets of model peptides, G−G−X−A−G−G and G−G−X−P−G−G (*49*, *50*). Similarly, we calculated the correction factor B of proline for H_α and found it to be -0.29 ± 0.02 ppm. When the preceding residue of proline is glycine, the correction factors obtained from peptides G−G−X−G−G are still valid since there is no approximation in this case, i.e., the factor B is −0.6 ppm for C_α and −0.11 ppm for H_α, respectively.

Figure 2 shows the corrected chemical shift deviations from the random coil shifts. The C_α chemical shifts are significantly larger than the random coil shifts for the region G25−A42, indicating the presence of residual α-helical structures for this fragment. Most of the residues outside this region show similar chemical shifts as random coil values. Residues I19 and D23 show significant upfield shifts, which

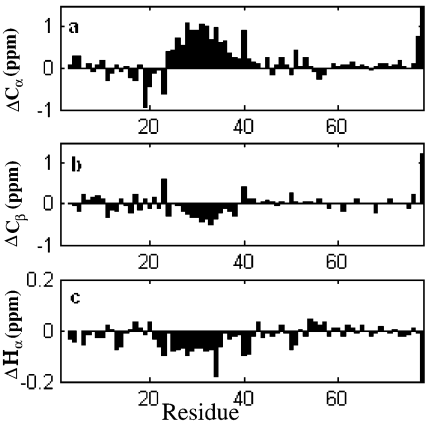

FIGURE 2: Deviation of chemical shifts C_α (a), C_β (b), and H_α (c) from the sequence-corrected random coil values.

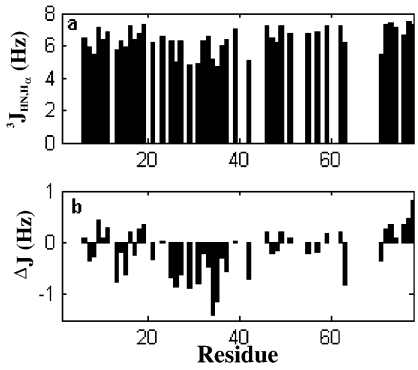

FIGURE 3: (a) $^3J_{HN,H\alpha}$ coupling constants derived from HNHA 3D experiments. (b) Deviation of the coupling constants from context-corrected statistical random coil values.

may result from an improper correction factor for proline residue. The chemical shift deviation for C_β (ΔC_β) is significantly less than ΔC_α. The negative ΔC_β values for G25−R38, however, also support the presence of α-helical propensities for residues in this region. Unlike C_α resonances, C_β resonances are shifted only slightly from random coil positions in helical structure (*48*), which explains for its relatively poor diagnostic capacity in the study of unfolded NG. Similar to ΔC_α and ΔC_β, the deviation of H_α chemical shifts from random coil values is negligible for most of the residues in C-terminal and N-terminal regions. The negative values of ΔH_α for residues P20−A42 further confirm the existence of an α-helical structure in this region. All the chemical shift data are consistent with the presence of a residual α-helical structure in the region from G25 to A42. The mean population of α-helix can be estimated by using helical secondary chemical shifts of 2.8 and −0.3 ppm for C_α and H_α (*48*), respectively. The resultant helical populations for the fragment G25−A42 were 22 and 28% as calculated from C_α and H_α chemical shifts, respectively.

$^3J_{HNH\alpha}$ Coupling Constants. Three-bond J coupling constants are sensitive to dihedral angle Φ and provide valuable information about secondary structure. $^3J_{HNH\alpha}$ values which significantly deviated from random coil values (6−7.5 Hz) indicate definite propensities for the secondary structures. Figure 3a shows the experimental results. The *J* values for several residues could not be obtained accurately due to resonance overlap. Similar to chemical shifts, the random coil *J* values of all amino acids were corrected for local effect since its coupling constant value is affected by its preceding residue (*51*, *52*). The random coil *J* value for glycine residue given in the literature (*52*) (5.9 Hz) is smaller than what we expected. There are 18 glycine residues in NG, and most of them are in the random coil state as indicated by chemical shifts. Therefore, the average *J* value (7.0 ± 0.2 Hz) over 14 glycine residues located at the C terminal region, G55−D78, is used as a reference for random coil coupling constant. The deviation of coupling constants from the corrected coil values is shown in Figure 3b. The coupling constants for residues in the region from L21−A42 are significantly smaller than the random coil values, supporting the argument that G25−A42 preferentially populate the α-region of (ϕ, ψ) space.

Homonuclear NOEs. $^1H-^1H$ NOE is another indicator of the presence of residual structures for unfolded proteins. We measured homonuclear NOEs using ^{15}N-edited NOESY−HSQC experiments. The NOE connectivities and their relative intensities are shown in Figure 4. Strong or medium $d_{\alpha N(i,\ i+1)}$ NOEs are observed for most of the residues in the N-terminal region E6−G49, while weak $d_{\alpha N(i,\ i+1)}$ NOEs are observed for the residues in the C-terminal region, indicating the high mobility of this part. $d_{NN(i,i+1)}$ NOEs for two regions G25−S36 and D15−D18 are observed. The relative intensities of the sequential $d_{\alpha N(i,\ i+1)}$ and $d_{NN(i,i+1)}$ NOEs provide an estimation of the relative population of backbone dihedral angles at each residue in the α- and β-regions of the conformational (ϕ, ψ) space. The region D15−D18 displays the smallest $d_{NN(i,i+1)}/d_{\alpha N(i,\ i+1)}$ ratio (<0.3), indicating the existence of a very small population of α-conformations in this part of the sequence. The population of the α-conformations is so small that it is undetectable by chemical shifts and *J* couplings (Figures 2−4). In the region of G25−K32, the ratio $d_{NN(i,i+1)}/d_{\alpha N(i,\ i+1)}$ is apparently large (∼1.0), implying that this part of the sequence has the highest population of dihedral angles in the α-region of the (ϕ, ψ) space. The relatively smaller sequential NOE ratios in the region I33−S36 indicate that this fragment samples both the α- and β-regions of the conformational space, but the population of α-conformations is lower than the fragment G25−K32. Although chemical shifts and *J* coupling constants indicate the presence of residual structure in the region G25−S36, no medium-range NOEs such as $d_{NN(i,i+2)}$ were detected. One possibility is that the residual structure undergoes rapid exchange with random coil conformers. Thus, insufficient amount of stable α-helical structure exists to give rise to detectable medium- or long-range NOEs.

Hydrogen exchange rate between amide and water protons depends on the degree of exposure of the amide proton to solvent. For random coil, the residence time of the amide protons is in the order of milliseconds. On the other hand, the residence time can be much longer (seconds to weeks) for amide protons involved in hydrogen bonds in regular secondary structures. The cross-peaks between water protons and amide protons observed in the NOESY−HSQC spectrum result from water-amide proton exchange. The water NOESY peak intensities shown in Figure 4 provide a rough estimation of the relative exchange rates. The weaker the exchange peak intensity (d_{NH,H_2O}) is, the larger the protection factor (*53*) is. Residues located at regions G25−Q34 show small exchange rates, indicating that they are less accessible to solvent as a result of residual structure formation. Consistent with this,

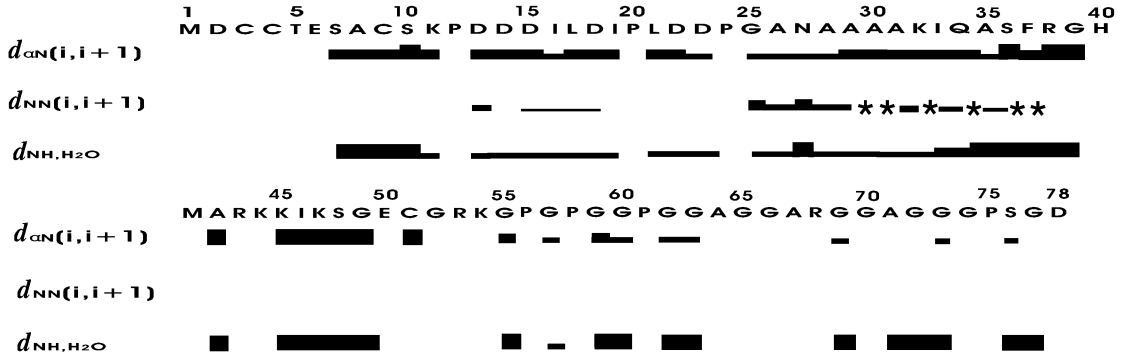

FIGURE 4: Relative intensities of $^1H_\alpha(i)-^1H_N(i+1)$ NOE ($d_{\alpha N(i,i+1)}$), $^1H_N(i)-^1H_N(i+1)$ NOE ($d_{NN(i,i+1)}$), $^1H_N-H_2O$ chemical exchange ($d_{NH,H2O}$). The thickness of the bars represents the estimated relative NOE or exchange peak intensity (strong, medium, weak). NOEs that are obscured due to overlapping resonance are indicated by asterisks (*).

the amide proton temperature coefficients in this region are also significantly smaller than the rest of the sequence. The average values are -5.7 ± 1.5 ppb/K for G25-Q34 and -8.5 ± 1.0 ppb/K for the rest of the residues in the sequence. It has been found that amide located in hydrogen-bonded regular secondary structure displays a more positive proton temperature coefficient than −4.5 ppb/K (*54*), while amide located in random coil shows a more negative coefficient than −8.0 ppb/K (*53*, *55*). Therefore, a small amount of cooperatively folded α-helix might exist in the region G25−Q34.

Residues D15−D18 display weak exchange peaks in the HQSC−NOESY spectrum, but their amide proton temperature coefficients are more negative than −8.0 ppb/K. Except for the amide proton exchange rate, other factors such as amide proton relaxation and water suppression can influence the exchange peak intensity. The C-terminal residue D78 should not be involved in backbone hydrogen bonding interaction. Its temperature coefficient is −7.6 ppb/K, but its exchange peak is very weak. Hence, amides with very fast exchange rates may give very weak exchange peaks. According to chemical shifts, sequential NOEs and temperature coefficients, the region D15−D18 is in a random coil state with a slight preference toward the α-region of conformational space.

It is interesting to observe that residues around S36 (A35−A42) show relatively large water−amide exchange rates and large negative proton temperature coefficients. In addition, with the information of chemical shifts (Figure 2), we can argue that the region surrounding the phosphorylation site (S36) populates the α-region of the (ϕ, ψ) space but do not form folded secondary structure. A previous study using a peptide corresponding to residues A30−K45 of rat NG showed that the peptide has a tendency to form an α-helix in the region surrounding the phosphorylation site (*18*). The region F37−G39 was proposed to form a folded structure in aqueous solution (*18*). Due to the lack of a number of residues ($A_{26}N_{27}A_{28}A_{29}$) with high α-helix propensity at the N-terminus of the peptide, the peptide forms a less stable helical structure in the N-terminal region A30−Q34 compared to the full-length protein. Although residues F37−G39 are located in the middle of the peptide, interestingly, their structures can still be affected by additional amino acids at both termini of the peptide as evidenced by the structural difference between the peptide and full-length protein. The region surrounding the phosphorylation site adopts a fluid

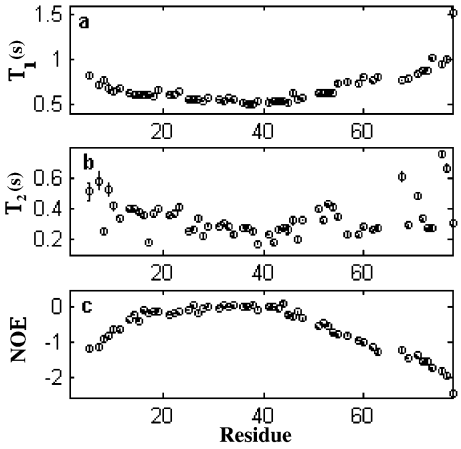

FIGURE 5: Relaxation times T_1 (a) and T_2 (b) and heteronuclear $^1H-^{15}N$ NOE (c).

structure, and this may allow PKC to access this site more easily and facilitate the catalysis process.

Relaxation Properties of NG. The relaxation parameters T_1, $T_{1\rho}$, and heteronuclear NOE were measured for all detectable backbone amides in NG. Unambiguous intensity measurements were possible for resonances from 56 of the 71 nonproline residues. T_2 was calculated from $T_{1\rho}$ and T_1. Figure 5 is a plot of T_1, T_2, and the heteronuclear NOE for these residues. Relaxation time T_1 gradually decreases with distance from the termini and then reaches a plateau formed between residues D13 and S48, forming an upside-down bell-shape profile. Interestingly, the profile is asymmetric around the center of the protein sequence, while a symmetrical profile is expected for a random coil polypeptide (*56*). In NG, most of the residues in the N-terminal half of the protein are located at the plateau. Similarly, the distribution of heteronuclear NOEs along the amino acid sequence displays an asymmetric bell-shape profile. The NOE values for the residues in the plateau are about zero, while others are negative, indicating that residues between D13−S48 form a relatively compact structure instead of a random coil. Relaxation time T_2 follows a similar profile as T_1 does. However, unlike T_1 and NOE, T_2 values show significantly local variations along the sequence, especially for residues in the C-terminal domain. Such local variations result from slow motions on the millisecond to microsecond time scale.

Spectral Density Analysis. The values of the spectral density functions for NG were calculated and are illustrated in Figure 6. The flexibility along the protein backbone can

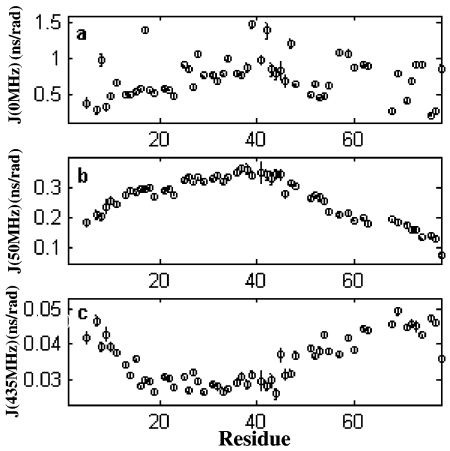

FIGURE 6: Spectral density function J(0) (a), J(ω_N) (b), and J(0.87ω_H) (c) derived from relaxation data.

be characterized by correlating the spectral density values with the protein sequence. Spectral density parameters $J(0)$, $J(\omega_N)$, and $J(\omega_H)$ indicate that the region between D15 and S48 is more restricted than other residues. The increase in $J(0)$ for the C-terminal region G55−D78 arises from an increase in molecular motions on the microsecond to millisecond time scale. Similarly, the abnormal $J(0)$ values for residues A8, L17, G39, A42, and K47 result from slow backbone motions.

Unfolded proteins in which there is little ordered structure are characterized by relatively uniform backbone dynamics and small $J(0)$ values that are nearly equal to $J(\omega_N)$. For example, the unfolded apo-plastocyanin (99 residues) under nondenaturing conditions at 35 °C has a $J(0)$ value of about 0.3 ns/rad and $J(\omega_N)$ values of about 0.2 ns/rad (*57*). On the other hand, unfolded proteins with significant amount of ordered structure show nonuniform backbone dynamics and much larger $J(0)$ values and a substantial difference between $J(0)$ and $J(\omega_N)$. For example, unfolded drk SH3 domain (61 residues), which possesses a significant amount of residual structure, shows a gradual decrease of $J(0)$ values at increasing positions toward both termini. The $J(0)$ values (∼1.0 ns/rad) are much larger than $J(\omega_N)$ (∼0.3 ns/rad) values for the residues in the middle of the SH3 sequence (*58*). The spectral density profiles of NG (Figure 6) are quite different from those with little residual structures, but similar to the drk SH3 domain. This further confirms the conclusion drawn from secondary chemical shifts and J coupling constants. Spectral density parameters indicate that residues between D15 and S48 move collectively in certain degrees. For a folded protein with about 75 residues, the overall rotational correlation time is about 4 ns at 25 °C, corresponding to a maximum $J(0)$ of 1.6 ns/rad and a maximum $J(\omega_N)$ of 0.62 ns/rad. Most of the residues within the region G25−A42 display $J(0)$ values of ∼0.8 ns/rad (Figure 6), corresponding to local correlation times of ∼2 ns. The $J(0)$ and $J(\omega_N)$ values of NG (Figure 6) show that the protein is still quite flexible although about 20% α-helical structure exists in the region G25−A42.

Model-Free Analysis. Our previous study demonstrated that order parameters for unfolded proteins can be extracted according to eq 4 (*43*). In this case, an apparent local correlation time was applied to each residue although a global correlation time is no longer valid. The calculated values of

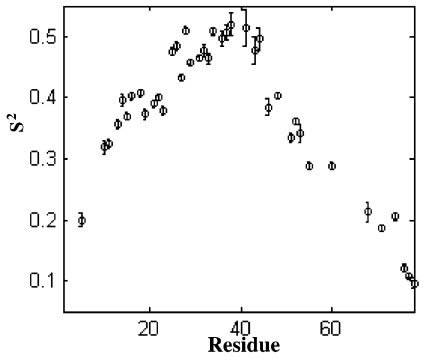

FIGURE 7: Square of order parameters (S^2) derived from relaxation data

S^2 are shown in Figure 7. To estimate the effect of slow exchange process (R_{ex}) on the accuracy of calculating S^2, we did similar simulations as described previously (*43*), with the exception that R_{ex} was added to the synthesized transverse relaxation rate ($1/T_2$). When $S^2 < 0.5$, the error in the resultant S^2 is still less than 10% in the case where $\tau_e' < 0.15$ ns. Thus, several residues with large R_{ex} that showed $\tau_e' > 0.15$ ns were excluded from Figure 7. The average S^2 values were 0.48 ± 0.02 for residues G25−K44, 0.39 ± 0.02 for residues D15−D23, and 0.36 ± 0.03 for the region from I46 to R53. The order parameters for the residues in the C-terminal domain (G55−D78) were less than 0.3 (average value 0.22 ± 0.07, many data are not shown in Figure 7 due to large τ_e' values). S^2 describes the degree of motional restriction and a value of 1 corresponds to completely rigidity while a value of zero corresponds to no restriction. Therefore, the order parameters support the conclusion that the region from D15 to S48 is relatively rigid and moves collectively in a certain degree.

NG−CaM Interaction. In the CaM titration of ^{15}N-labeled NG (NG protein concentration of 0.7 mM, pH 6.5, 50 mM KH_2PO_4 buffer, 5 mM DTT, 5 mM EGTA, at 25 °C), many cross-peaks in the ^{1}H−^{15}N HSQC spectrum showed gradual decreases in intensity and no significant changes of positions with increases of CaM concentration. Finally, most of the peaks disappeared and several new weak cross-peaks appeared in the HSQC spectrum. Even at a CaM/NG ratio of 2.5:1, most residues in the region D15−C51 were not observed. The diminishing of peaks is not because the complex is more rigid and larger than the free NG, but is a result of very weak binding between the two proteins. In this case, NG can exchange between free and complex states and has significant populations in both states. Previous studies showed that the binding affinity between the reduced NG and CaM was 5.4 μM at pH 7.2, 100 mM NaCl, and 2 mM EGTA as determined by CD spectroscopy, while the affinity between the CaM and an NG mutant was 2.9 and 14 μM, respectively, as determined by CD spectroscopy and sedimentation equilibrium. Our NMR results however show that the dissociation constant for the reduced form is much larger than 5 μM.

If the exchange occurs at a time scale of milliseconds to microseconds, an amide may not be detectable in the HSQC spectrum when the chemical shifts of its ^{1}H and/or ^{15}N are different in both states. The disappearance of a cross-peak is a good indication of the corresponding residue involved in binding and/or undergoing significant structural changes.

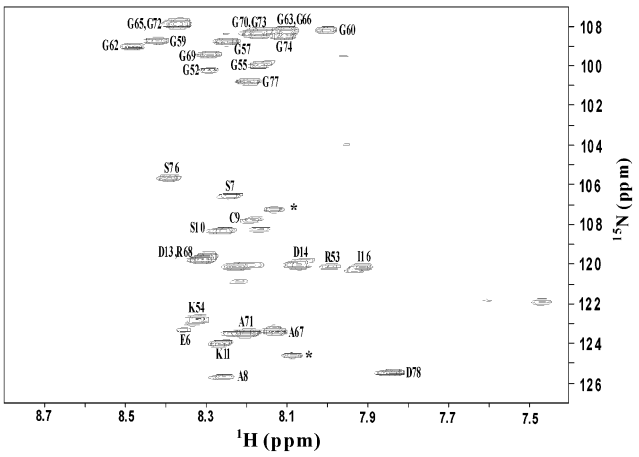

FIGURE 8: $^{1}H-^{15}N$ heteronuclear single quantum correlation spectrum (HSQC) of neurogranin−CaM complex recorded at 25 °C. The resonance assignments are indicated by amino acid names followed by residue numbers. Resonances resulting from impurities are indicated by asterisks (*).

Figure 8 shows the $^{1}H-^{15}N$ spectrum of the complex at respective protein concentrations of 0.7 mM for NG and 1.75 mM for CaM, pH 6.5, 50 mM KH_2PO_4 buffer, 5 mM EGTA, 5 mM DTT, at 25 °C. The resonance assignment was confirmed by HNCACO and HNCOCA spectra. In comparison with the spectrum of the free NG form (Figure 1), the highly flexible terminal parts R53−D78 and E6−D13 remains unchanged upon binding to CaM. Most of residues in the region D15−G52 do not give signals in the HSQC spectrum. Several residues in this region show weak signals with shift positions. The results indicate that residues D15−G52 in NG undergo significant structural changes upon binding to CaM.

Gerendasy et al. studied nine peptides (NG_{1-20}, NG_{12-24}, NG_{16-42}, NG_{25-47}, NG_{34-51}, NG_{40-55}, NG_{44-54}, NG_{55-66}, and NG_{66-78}) that cumulatively span the entire amino acid sequence of NG and their interactions with CaM, using CD spectroscopy. It was concluded that CaM stabilizes an amphiphilic α-helix within NG (G25−K47) in the absence of Ca^{2+} (*8*). A highly basic stretch of residues R43−K47 outside the IQ domain was identified to be crucial CaM-binding residues (*8*). In addition, I33, S36, and R38 within the IQ domain were found to be important for CaM binding to NG in vivo (*59*). From our NMR results, we could not define which residues were involved in the binding sites. However, it is clear that besides the IQ domain many residues (D15−K32 and K44−G52) are involved in the interaction with CaM or undergo significant structural changes. G52 is still visible in Figure 8, but its chemical shifts change significantly upon binding CaM.

Implication for Protein−Protein Interaction and Complex Stability. The interaction between NG and CaM has been considered to be mediated through the IQ domain. The IQ domain plus nine residues consecutive to the N-terminus of the IQ motif have a greater propensity to form an α-helix. As found in many IQ motifs, the hydrophobic and basic residues along the putative α-helix exhibit a characteristic pattern. A patch of hydrophobic residues (I33, F37, M41, and A42 in NG) is found on one side of the helix, while a patch of positively charged residues (K32, H40, R43, K44, and K45) is found on the opposite side. Membrane (micelle) can stabilize the helix through hydrophobic interactions between the membrane and hydrophobic residues in the IQ domain (*18*). Recently, a structural model of apo-CaM binding to the first IQ motif in an unconventional myosin was built (*60*). The model revealed that polar residues in the IQ motif participate in the formation of many hydrogen bonds with residues of CaM (*60*). On the other hand, the hydrophobic residues within the IQ motif (corresponding to the first, fifth, and eighth residues in the consensus sequence) interact with the apolar interior of the semi-open C-terminal lobe of CaM (*60*). For NG, the continuous hydrophobic surface formed by the residues within the IQ domain can be extended to A30 and then to A26 in an α-helical structure conformation. The hydrophobic surface might signal the position of the C- and N-terminal lobes of CaM as they wrap around the NG. Although the α-helix in the region G25−A42 is nascent, the probability of finding a continuous hydrophobic surface in such a nascent structure is lower than in a stable α-helix, but much higher than in a random coil state. Therefore, the existence of a nascent helical structure facilitates the recognition of NG by CaM.

The detail of the structural rearrangement that occurs, when NG binds to its partner, is not clear. However, the apparent change in conformational entropy of many of the residues involved in binding is significant. Such entropy change will play a critical role in determining the strength of protein−protein interaction. We have recently developed an approach for predicting conformational entropy change between conformational states based on NMR derived order parameters (*61*). When S^2 is smaller than 0.95, the prediction method is applicable. It is important to note that the predicted entropy change reflects only changes in rapid motions visible by NMR relaxation. Of course, additional contributions from slow motions, collective motions, bonds other than N−H vectors and solvent will be involved in the net entropy change. For drk SH3 domain, the average entropy change between the folded and partially unfolded states was about 12 J/mol K per residue. Although the prediction method is oversimplified, this value is very similar to what has been estimated for protein folding using a number of techniques (*62*). The average S^2 values were 0.36 ± 0.03, 0.48 ± 0.02, and 0.39 ± 0.02 for regions D15−D23, G25−K44, and I46−G52, respectively. Assuming an NH S^2 value of 0.85 for the residues located in binding regions in the NG−CaM complex, we predicted that the conformational entropy changes were 14.3 ± 0.4, 11.9 ± 0.4, 13.7 ± 0.4 J/mol K per residue for the three regions D15−D23, G25−K44, and I46−R53 upon NG binding to CaM. Assuming that entropy is additive, the energy cost for immobilizing the residues in region D15−G52 will be about 146.3 kJ/mol at 25 °C. From the simple calculation, we can see that the entropic cost for NG residues rigidly held by CaM is tremendous. This can account for the instability of the complex. If this region is as flexible as the C-terminal domain residues ($S^2 = 0.22$), immobilization of the same fragment will cost 192.6 kJ/mol at 25 °C. The presence of a nascent helical structure in the region G25−A42 of free NG significantly reduces the energy cost for forming protein−protein complex, and thus NG can bind to CaM. At the same time, the flexibility of the unfolded NG allows it to interact with different proteins such as CaM, PKC, and possibly some other unknown proteins.

ACKNOWLEDGMENT

We thank Dr. Mitsu Ikura, Ontario Cancer Institute, University of Toronto, Canada for providing the plasmid used in the expression of the CaM. We are grateful to Dr. Yu-Keung Mok for his critical evaluation of the manuscript. The authors also thank Ms. Peggy Ler for proofreading the manuscript.

REFERENCES

1. Gerendasy, D. D., and Sutcliffe, J. G. (1997) *Mol. Neurobiol. 15*, 131−163.
2. Neuner_Jehle, M., Denizot, J. P., and Mallet, J. (1996) *Brain Res. 733*, 149−154.
3. Ramakers, G. M., Gerendasy, D. D., and Graan, P. N. D. (1999) *J. Biol. Chem. 274*, 1873−1874.
4. Baudier, J., Deloulme, J. C., VanDorsselaer, A., Black, D., and Matthes, H. W. D. (1991) *J. Biol. Chem. 266*, 229−237.
5. Huang, K. P., Huang, F. L., and Chen, H. C. (1993) *Arch. Biochem. Biophys. 305*, 570−580.
6. Cox, J. A., Comte, M., Fitton, J. E., and DeGrado, W. F. (1985) *J. Biol. Chem. 260*, 2527−2534.
7. Crivici, A., and Ikura, M. (1995) *Annu. Rev. Biophys. Struct. 24*, 85−116.
8. Gerendasy, D. D., Herron, S. R., Jennings, P. A., and Scutcliffe, J. G. (1995) *J. Biol. Chem. 270*, 6741−6750.
9. Bahler, M., and Rhoads, A. (2002) *FEBS Lett. 513*, 107−113.
10. Cheney, R. E., and Mooseker, M. S. (1992) *Curr. Opin. Cell Biol. 4*, 27−35.
11. Xie, X., Harrison, D. H., Schlichting, I., Sweet, R. M., Kalabokis, V. N., Szent-Gyorgyi, A. G., and Cohen, C. (1994) *Nature 368*, 306−312.
12. Block, S. M. (1996) *Cell 87*, 151−157.
13. Hayashi, N., Matsubara, M., Titani, K., and Taniguchi, H. (1997) *J. Biol. Chem. 272*, 7639−7645.
14. Watson, J. B., Szijan, I., and Coulter, P. M. (1994) *Mol. Brain Res.*, 323−328.
15. Chapman, E. R., Au, D., Alexander, K. A., Nicolson, T. A., and Storm, D. R. (1991) *J. Biol. Chem. 266*, 207−213.
16. Houbre, D., Duportail, G., Deloulme, J. C., and Baudier, J. (1991) *J. Biol. Chem. 266*, 7121−7131.
17. Paudel, H. K., Zwiers, H., and Wang, H. J. (1993) *J. Biol. Chem. 268*, 6207−6213.
18. Chang, D. K., Chien, W. J., and Arunkumar, A. I. (1997) *Biophys. J. 72*, 554−566.
19. Krucker, T., Siggins, G. R., McNamara, R. K., Lindsley, K. A., Dao, A., Allison, D. W., Lecea, L., Lovenberg, T. W., Sutcliffe, J. G., and Gerendasy, D. D. (2002) *J. Neurosci. 22*, 5525−5535.
20. Sheu, F. S., Mahoney, C. W., Seki, K., and Huang, K. P. (1996) *J. Biol. Chem. 271*, 22407−22413.
21. Mahoney, C. W., Pak, J. H., and Huang, K. P. (1996) *J. Biol. Chem. 271*, 28798−28804.
22. Li, J., Pak, J. K., and Huang, K. P. (1999) *J. Biol. Chem. 274*, 1294−1300.
23. Martzen, M. R., and Slemmon, J. R. (1995) *J. Neurochem. 64*, 92−100.
24. Slemmon, J. R., and Martzen, M. R. (1994) *Biochemistry 33*, 5653−5660.
25. Huang, K. P., Huang, F. L., Li, J. F., Schuck, P., and McPhie, P. (2000) *Biochemistry 39*, 7291−7299.
26. Cho, H. S., Liu, C. W., Damberger, F. F., Pelton, J. G., Nelson, H. C. M., and Wemmer, D. E. (1996) *Protein Sci. 5*, 262−269.
27. Sem, D. S., Casimiro, D. R., Kliewer, S. A., Provencal, J., Evans, R. E., and Wright, P. M. (1997) *J. Biol. Chem. 272*, 18038−18043.
28. Schulz, G. E. (1979) *Molecular Mechanisms of Biological Recognition*, Elsevier/North-Holland Biomedical Press, Amsterdam, The Netherlands.
29. Spolar, R. S., and Record, M. T. J. (1994) *Science 263*, 777−784.
30. Lu, P. J., and Chen, C. S. (1997) *J. Biol. Chem. 272*, 466−472.
31. Miao, H. H., Ye, J. S., Wong, S. L. Y., Wang, B. X., Li, X. Y., and Sheu, F. S. (2000) *Bioelectrochemistry 51*, 163−173.
32. Ikura, M., Kay, L. E., and Bax, A. (1990) *Biochemistry 29*, 4659−4667.
33. Wittekind, M., and Mueller, L. (1993) *J. Magn. Reson. 101*, 201−205.
34. Grzesiek, S., and Bax, A. (1993) *J. Am. Chem. Soc. 115*, 12593−12594.
35. Muhandiram, D. R., and Kay, L. E. (1994) *J. Magn. Reson. Ser. B 103*, 203-216.
36. Kuboniwa, H., Grzesiek, S., Delaglio, F., and Bax, A. (1994) *J. Biomol. NMR 4*, 871−878.
37. Zhang, O., Kay, L. E., Olivier, J. P., and Forman-Kay, J. D. (1994) *J. Biomol. NMR 4*, 845−858.
38. Montelione, G. T., Lyons, B. A., Emerson, S. D., and Tashiro, M. (1992) *J. Am. Chem. Soc. 114*, 10974−75.
39. Delaglio, F., Grzesiek, S., Vuister, G. W., Zhu, G., Pfeifer, J., and Bax, A. (1995) *J. Biomol. NMR 6*, 277−293.
40. Farrow, N. A., Zhang, O., Forman-Kay, J. D., and Kay, L. E. (1995) *Biochemistry 1995*, 868−878.
41. Akke, M., and Palmer, A. G. (1996) *J. Am. Chem. Soc. 118*, 911−912.
42. Farrow, N. A., Zhang, O., Forman-Kay, J. D., and Kay, L. E. (1995) *J. Biomol. NMR 6*, 153−162.
43. Yang, D. W., Mok, Y. K., Forman-Kay, J. D., Farrow, N. A., and Kay, L. E. (1997) *J. Mol. Biol. 272*, 790−804.
44. Schurr, J. M., Babcock, H. P., and Fujimoto, B. S. (1994) *J. Magn. Reson. Ser. B 105*, 211−224.
45. Alexandrescu, A. T., and Shortle, D. (1994) *J. Mol. Biol. 242*, 527−546.
46. Lipari, G., and Szabo, A. (1982) *J. Am. Chem. Soc. 104*, 4546−4559.
47. Wishart, D. S., Sykes, B. D., and Richard, F. M. (1991) *J. Mol. Biol. 222*, 311−333.
48. Wishart, D. S., and Sykes, B. D. (1994) *Methods Enzymol 239*, 363−392.
49. Wishart, D. S., Bigam, C. G., Holm, A., Hodges, R. S., and Sykes, B. D. (1995) *J. Biomol. NMR 5*, 67−81.
50. Schwarzinger, S., Kroon, G. J. A., Foss, T. R., Chung, J., Wright, P. E., and Dyson, H. J. (2001) *J. Am. Chem. Soc. 123*, 2970−2978.
51. Penkett, C. J., Redfield, C., Dodd, I., Hubbard, J., McBay, D. L., Mossakowska, D. E., Smith, R. A. G., Dobson, C. M., and Smith, L. J. (1997) *J. Mol. Biol. 274*, 152−159.
52. Smith, L. J., Bolin, K. A., Schwalbe, H., MacArthur, M. W., Thornton, J. M., and Dobson, C. M. (1996) *J. Mol. Biol. 255*, 494−506.
53. Yao, J., Chung, J., Eliezer, D., Wright, P. E., and Dyson, H. J. (2001) *Biochemistry 40*, 3561−3571.
54. Baxter, N. J., and Williamson, M. P. (1997) *J. Biomol. NMR 9*, 359−369.
55. Waltho, J. P., Feher, V. A., Merutka, G., Dyson, H. J., and Wright, P. E. (1993) *Biochemistry 32*, 6337−6347.
56. Hu, Y., Maclnnis, J. M., Cherayil, B. J., Fleming, G. R., Freed, K. F., and Perico, A. (1990) *J. Chem. Phys. 93*, 822−836.
57. Bai, Y., Chung, J., Dyson, H. J., and Wright, P. E. (2001) *Protein Sci. 10*, 1056−1066.
58. Farrow, N. A., Zhang, O., Forman-Kay, J. D., and Kay, L. E. (1997) *Biochemistry 36*, 2390−2402.
59. Prichard, L., Deloulme, J. C., and Storm, D. R. (1999) *J. Biol. Chem. 274*, 7689−7694.
60. Houdusse, A., Silver, M., and Cohen, C. (1996) *Structure 4*, 1475−1490.
61. Yang, D. W., and Kay, L. E. (1996) *J. Mol. Biol. 263*, 369−382.
62. Doig, A. J., and Sternberg, M. J. E. (1995) *Protein Sci. 4*, 2247−2251.

BI0271751